Integrated geophysical approach in assessing karst presence and sinkhole susceptibility along flood-protection dykes of the Loire River, Orléans, France

Kevin Samyn, Francis Mathieu, Adnand Bitri, Aude Nachbaur, Luc Closset

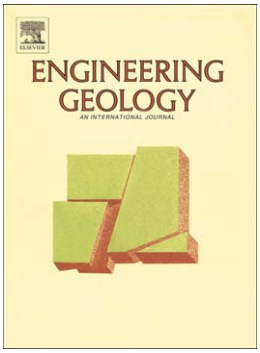

Integrated geophysical approach in assessing karst presence and sinkhole susceptibility along flood-protection dykes of the Loire River, Orléans, France

K. Samyn, F. Mathieu, A. Bitri, A. Nachbaur, L. Closset

PII: S0013-7952(14)00268-3
DOI: doi: 10.1016/j.enggeo.2014.10.013
Reference: ENGEO 3900

To appear in: *Engineering Geology*

Received date: 6 January 2014
Revised date: 22 September 2014
Accepted date: 13 October 2014

Please cite this article as: Samyn, K., Mathieu, F., Bitri, A., Nachbaur, A., Closset, L., Integrated geophysical approach in assessing karst presence and sinkhole susceptibility along flood-protection dykes of the Loire River, Orléans, France, *Engineering Geology* (2014), doi: 10.1016/j.enggeo.2014.10.013

Integrated geophysical approach in assessing karst presence and sinkhole susceptibility along flood-protection dykes of the Loire River, Orléans, France.

K. Samyn[a*], F. Mathieu[a], A. Bitri[a], A. Nachbaur[a], L. Closset[a]

[a] BRGM, Bureau de recherches géologiques et minières, France. 3 Avenue Claude Guillemin BP36009 45060 Orléans Cedex 2, France.

[*] Corresponding author. Tel: +33 (0)2 38 64 34 54; fax: +33 (0)2 38 64 36 89. E-mail address: k.samyn@brgm.fr

Abstract

Non-invasive geophysical methods are often used for detecting near-surface defects and monitoring seepage in river dykes or dams. Between 2008 and 2009, a series of geophysical experiments were conducted to detect karst features below the dykes of the Loire River, Orléans, France. Multi-channel analysis of seismic surface waves (MASW) was used to obtain the shear wave velocity (Vs) profile of the subsurface below the dykes. As an effective approach for investigating the structure of the dykes, multi-channel resistivity surveys were also used to evaluate the electrical properties of material inside and under the dykes. This study discusses the exploration strategy and results for several sections of the dyke system. Based on the experimental data, Vs contours are used to geometrically and qualitatively describe the subsurface under the dykes and identify areas of mechanical weakness corresponding to karst features, while resistivity contours allow distinguishing interactions between karst and the dykes through the identification of areas of downward material movement. Known and unknown anomalies are identified. A practical approach that combines seismic and electric resistivity results is proposed to assess karst presence and

sinkhole hazard along the investigated dykes using a susceptibility index referring to the likelihood level of the events. As a validation method, areas of strong karst susceptibility index along the dykes are compared to known collapse event (sinkholes, dyke breaches etc.) locations, available in databases.

Keywords

River dyke; seismic surface waves; electrical resistivity tomography; sinkhole; karst

1. Introduction

Shallow karst constitute a serious hazard for the public and existing construction due to the risk of sinkhole development and subsidence, which can cause damage and increase the costs of urban development. Detecting karst features, voids, surficial dissolution, fissuring, alteration and unconsolidated material by geophysical techniques is thus a major challenge for many infrastructure managers. As a matter of fact, reliable characterization of the dyke material are required for the verification of its stability. The importance of an observation of dyke stability became obvious in the light of major flood events, such as the Elbe flood of 2002 in central Europe. Survey campaigns on dykes often focus on geotechnical parameters obtained in situ by standard penetration and cone penetration tests, or in the laboratory based on borehole samples. A disadvantage of these tests is their selective character. An extensive number of tests are required to cover a dyke sufficiently. On the other hand, most non-destructive geophysical methods are able to survey large areas effectively. The dykes that were the subject of this study are located approximately 100 km south of Paris, on the banks of the Loire River, and are built on the highly karstified calcareous Beauce Formation of Aquitainian age substratum. As evidence of this, the Loiret springs are amongst the most important karst springs in France, and sinkholes regularly occur in their vicinity. These cavities were also the cause of unforeseen expenses during the construction of a tramway line and a bridge over the Loire River. Geophysical measurements conducted on the Loire River dykes are integrated into a general approach that aims to assess karst hazards. Karst systems are characterised by complex geomorphology and hydrology (Ford and Williams, 2007). Voids can take the form of large cavities, super-imposed conduits and networks of open fractures or micrometric fissures. Karstification is commonly revealed by surficial features; in the uppermost layer of karstified zones, dissolution by meteoric water can enlarge fissures, thereby creating a zone of rapid infiltration filled with weathered, fractured and

unconsolidated material, or epikarst. Epikarst development can cause sinkhole phenomena draining surface materials (Palmer, 1991; Gunn, 2004). Some dangerous segments of the dykes need to be rebuilt, and others need to be strengthened. Because the nature and structure of the materials under the dykes vary from place to place, decisions about their treatment should first be supported by an understanding of the in situ subsurface conditions. The application of near-surface geophysics to river dyke characterisation has been studied in the past and has shown great promise (Bitri et al., 2010; Chen et al., 2006; Karl et al., 2011). A program to evaluate the condition of river dykes, supported by the local Regional Environment Department (DREAL), was executed from 2006 to 2011. The French Geological Survey (BRGM) and the DREAL funded a singular project to evaluate the probability of karst presence and the sinkhole susceptibility using a methodology based on a geophysical survey, under the dykes of the Loire River. The purpose of the project was therefore quite innovative as geophysical methodologies are usually used to characterize known hazardous events rather than try to predict them. Geophysical surveys covered a total length of more than 90 km of dykes with expected high probability of karst presence (Donsimoni et al., 2008). The complexity of karst features produces multiple and time-variable geophysical signatures. Shear-wave velocity and resistivity are known to be very good indicators of the degree of weathering and fissuring of a draining or saturated epikarst, and electrical behaviour may be enhanced by the presence of shallow groundwater and strong water circulation. Providing that anthropogenic interference allows their use, electrical imagery is a proven method for indirectly detecting karst systems (Guerin and Benderitter, 1995; Ioannis et al., 2002; Kaufmann, 2000; Valois et al., 2010, 2011). However, the use of a combination of geophysical tools is always preferable for obtaining a better-constrained model of near-surface features (Chen et al., 2006). For example, the exploration of a karst network in the Swiss Jura was conducted by combining GPR, which provides a precise image

of most surficial voids and structures, with gravimetry, which is sensitive to the presence of deeper and more extensive heterogeneities (Beres et al., 2001). To fit the objective of the project, a survey coupling electrical resistivity tomography (ERT) and multichannel analysis of surface waves (MASW), suitable for providing evidence of areas of mechanical weakness (Debeglia et al., 2006; Ganji et al., 1997; Matthews et al., 1996; Leparoux et al., 2000; Park et al., 1998; Shtivelman, 2002), was therefore undertaken. Several anomalous zones indicating karst activities were detected with both geophysical methods used. Indices derived from a coupled empirical analyse of the geophysical parameters then allowed the assessment of a karst presence probability and a sinkhole susceptibility along the investigated dykes. Supplementary geotechnical and observational data acquired from databases were used for calibration and as a test of the methodology.

2. Experimental site

The geophysical surveys were carried out at the top of the Loire River flood-protection dykes, near the city of Orléans, France. Donsimoni et al. (2008) estimated the probability of karst presence over the entire Loire River and especially in this area (Fig. 1). In the light of this study, 90 km of dykes divided into 10 profiles with high probability of karst presence were then selected and investigated with geophysical surveys (Fig. 2). The geophysical data acquisition was realized in 2008 and spread over a period of one year. 50 destructive geotechnical boreholes were also available on the investigated segments at the top of the dykes, useful for the calibration of the geophysical responses. These boreholes are described in further sections and were, by courtesy, provided by the local French roads and bridges laboratory (LRPC, Blois). The synthesis of boreholes data allowed to highlight the local lithology classification consisting in the upper sediments made of siliceous and argillaceous alluvia, 5 to 10 m thick, overlying the calcareous Beauce Formation (Aquitainian age), in which significant karst dissolution features occur. Karstification has resulted in many surface depressions (pits, sinkholes) and irregularities in both the upper surface of the Beauce Formation and at the ground

surface (Fig. 3). These conduits, generally around 2 to 3 m wide by 1 to 3 m thick, plunge quite rapidly to depths of 15–20 m or more.

3. Methodology

3.1 Exploration strategy

Electrical resistivity tomography (ERT) has become widely used in environmental and engineering applications. The method is popular in the investigation of groundwater (e.g., Benson et al., 1997; Khair and Skokan, 1998; Saksa and Paananen, 1992; Sandberg, 1993) as well as monitoring leaks in dyke dams (e.g., Johansson and Dahlin, 1996; Sjödahl et al., 2003). A multi-channel data acquisition system is suitable for obtaining the variation of resistivity with depth, using different electrode configurations along a line. The ERT approach was used to delineate the resistivity profile of the dyke bodies, with the aim of characterising their structure and detecting near-surface features.

Dispersive phase velocities of surface waves can be inverted to obtain shear-wave velocities (Vs) (e.g., Aki and Richards, 1980). The Vs profile of near-surface materials is one of the key parameters required in engineering. Multi-channel analysis of surface waves (MASW) (Park et al., 1999; Xia et al., 1999) has shown great promise in detecting shallow voids and tunnels, mapping bedrock surfaces, and delineating fracture systems in rock (Miller et al., 1999; Xia et al., 1998, 2004). The Vs of materials is an indicator of the seismic stiffness of the material. Current improvements in data acquisition, processing, and inversion (e.g., Xia et al., 2002a, 2002b, 2002c, 2003, 2004, 2005) provide confidence in the assessment of Vs. In this study, the MASW approach was used to delineate the Vs profile of the dykes, with the aim of detecting mechanical weakness in the deep limestone caused by karstification.

3.2 ERT acquisition and processing

2D resistivity surveys were carried out using a CC resistivity meter, the OhmMapper (Geometrics Inc., CA, USA), which uses line antennas as its capacitive sensors to acquire apparent resistivity data. The only array implemented by the OhmMapper is a line electrode dipole-dipole array which can properly image disturbances associated to karst features due to a high spatial resolution (Dahlin and Zhou, 2004). However other arrays could also provide reliable results for this type of application but no towable acquisition device with capacitive sensors currently exists with other electrode arrays to provide an acceptable cost effectiveness ratio for such a large investigation area. The system is a capacitively coupled resistivity meter that measures the electrical properties of rock and soil without the cumbersome ground stakes used in traditional resistivity surveys. A simple coaxial cable array with transmitter and receiver sections was pulled along the ground by a four-wheel drive. Data collection is many times faster with this system than with systems using conventional DC resistivity, and the system allowed an acquisition rate of approximately 8 km/day. The emitter on the back is connected to the receiver by an electrically insulating rope. The value of the intensity of the current injected by the transmitter is transmitted to the receivers via Bluetooth. Each receiver measures an electric potential whose value is sent to the recorder, together with the amperage. The recorder stores data at a frequency set by the user. For each position of the transmitter, the electrical signal was simultaneously recorded by 4 receiver locations. Dipole receivers are connected to each other and transmit the measured potential to the recorder. The distance between transmitter and receiver, as well as the length of the transmitter and receiver dipoles, determines the investigation depth. In this experiment, the line antennas (electrodes) with a nominated length of 5 m were used for both the transmitter and receivers. Therefore, the dipole length of the line electrode array was 10 m. Four receivers were used in the measurement with a rope length of 5 m. The corresponding available dipole distances were

then 15 m, 20 m, 25 m and 30 m. The apparent resistivity data were first filtered, removing data with standard deviations higher than 3%. A visual inspection was then made to remove outlier data before being smoothed using X2IPI (Bobatchev, 2003) to reduce geological noise (Fig. 4a and b). The apparent resistivities were then inverted to a default depth of 12 m using Res2Dinv (Loke and Dahlin, 2002; Loke and Dahlin, 2003) to obtain inverted resistivity geoelectric cross-sections. Each model consisted of 9 horizontal layers. Inversions with five iterations, robust constraint and a vertical to horizontal flatness filter ratio of 0.3, yielded satisfactory convergence, as is indicated by an RMS error ranging between 0.86% and 4.8% between measured and modeled apparent resistivity values for all surveys. To avoid an over-interpretation of the results, inverted resistivity sections were systematically truncated to a depth properly constrained by data of 8 m which can therefore be regarded as a reliable depth for interpretation.

3.3 MASW acquisition and processing

Seismic data were acquired following a roll-along procedure. To increase the speed and efficiency of MASW data recording and to thereby keep acquisition costs down, a new type of multichannel seismic cable was designed and manufactured to reach an acquisition rate of approximately 3 km/day. It consists of 24 geophones, at fixed 2-m intervals. Each geophone is attached to a single self-orienting, gimbal-mounted, vertical geophone with a 10 Hz resonance frequency. To help ensure proper coupling, each gimbal geophone is housed in a heavy casing (~1 kg). To damp the motion of the sensor around its rotational axis, the inside of the casing is filled with viscous oil. The seismic cable is towed behind a vehicle. A 24-channel Geometrics Stratavizor seismograph was used to record the impact from a weight-drop electronic seismic source. The source-to-nearest-receiver offset was 4 m. Therefore, the total length of the seismic line was 50 m. The source stations were separated by 10 m

increments along the segments of the dykes. Various tests (van der Veen and Green, 1998) applying these techniques have demonstrated that high-quality data, comparable to planted spike geophone data, can be acquired with gimbal geophones (Fig. 4c). Each 24-trace shot gather was analysed with Surfseis v2.0 (Park et al., 1999), facilitating the use of MASW with continuous profiling techniques. The first step consists of determining the dispersion curve (i.e., the phase velocity variation versus frequency) for each shot. The curve is calculated by using the slant-stack method in a common-shot gather, followed by a 1D Fourier transform over the intercept time (McMechan and Yeldin, 1981; Moktar et al., 1988, Park et al., 1998). The dispersion curve is directly obtained by picking the maximum values of the fundamental propagation mode of the obtained spectrum (Fig. 4d). The frequency range of 8 to 60 Hz was globally obtained for the dispersion curves of the whole seismic survey. The phase velocity and the thickness of layers for each dispersion curve were inverted using a 10 layers model to obtain a 1D Vs (shear wave velocity) profile with depth. Different approaches have been proposed for the inversion procedure. The more widely used approach is the linearised iterative least-squares technique (Gabriels et al., 1987; Moktar et al., 1988; Socco and Strobbia 2004; Xia et al. 1999). The linearised iterative least-squares technique used here is adapted from Hermann (1987). The inversion was stopped when a satisfactory convergence was reached, as is indicated by a maximum accepted RMS error in phase velocity between calculated and measured dispersion curves of 5 m/s. By placing each 1-D Vs profile at a surface location corresponding to the middle of the receiver line, a 2-D surface versus depth Vs map is constructed through a kriging interpolation scheme.

4. Results of ERT

Thirty-five destructive geotechnical boreholes were performed on the investigated segments at the top of the dykes, allowing calibration of the electrical responses. Information on these

surveys was, by courtesy, provided by the local French roads and bridges laboratory (LRPC, Blois). The synthesis of these calibrations allowed development of a lithology classification based on the inverted resistivity. Resistivities below 75 Ohm.m were found to be in good overall agreement with a clayey silt lithology (A) encountered by boreholes (Fig. 5a). Resistivities ranging from 75 to 200 Ohm.m were found to be in good overall agreement with a clayey sand lithology (SA) with a slightly variable clay fraction (SAa+ or SAs+) (Fig. 5b). Finally, resistivities over 200 Ohm.m were found to be in good overall agreement with clean sand and gravel lithology, corresponding to the Loire River deposits (SG) (Fig. 5c).

Disorders within the dyke bodies have also been detected by sudden and large changes in resistivity. These resistivity anomalies are generally limited to a few hundred metres in size, the dimensions of which are consistent with historical breaches, whose average length was evaluated at 190 m (Lino et al., 1999). These resistivity anomalies are highlighted either by a conductor body (A or SA) in a resistant bank (SG) or, conversely, by a resistant body (SG) in a conductor bank (A or SA), and they have been compared to historical disorders available in the French National database of underground cavities (BD cavités). According to this comparison, the resistivity anomalies in the dyke body can have different origins, such as former breaches, sinkhole filling or former reinforcement works on the dykes. Figure 6 shows examples of such detected disorders in the dyke body.

Disorders affecting the base of the dykes (e.g., the alluvial cover) are also highlighted by sudden and large changes in resistivity. The extension of these resistivity anomalies is generally less than in the dyke bodies, roughly a dozen metres to a hundred metres long. These disorders are highlighted not only by a sudden change in resistivity but also by a turning-down pattern of the interface characterising the base of the dyke body. These anomalies are likely to correspond to areas of potential sediment flow toward a karst network. Figure 7 shows examples of this type of anomaly.

5. Results of MASW

Calibration of the MASW was made more difficult by the small number available destructive geotechnical boreholes (15) that reached the underlying karstified limestone. However, synthesis of these calibrations with available boreholes allowed development of a lithology classification based on the inverted Vs (Fig. 8). Vs ranging from 100 to 300 m/s was found to be in good overall agreement with the Loire River overburden deposits (Se) encountered by boreholes. Vs ranging from 300 to 450 m/s were found to be in good overall agreement with a strongly karstified marly limestone (CA). Vs ranging from 450 to 600 m/s was found to be in good overall agreement with a more competent limestone-marl (C). Finally, Vs greater than 600 m/s was found to be in good overall agreement with the competent limestone-marl bedrock (S).

This classification allowed karstified areas at the top of the marly limestone formations to be detected by sudden and significant decreases in Vs. These Vs anomalies are generally limited in dimension to a few hundred metres, revealing the presence of karst networks instead of isolated karst channels, and are in good overall agreement with historical karst-related surface disorders of the BD cavités. The associated low-velocity anomalies may be due to weathering of the medium (CA) because of karstification. Figure 9 shows examples of this type of anomaly.

6. Assessing probability of karst presence

As mentioned in the previous paragraph, potentially karstified areas are highlighted by a sudden drop in Vs, revealing mechanical weakness associated with karst weathering. The methodology for assessing the probability of karst presence is then based on a step-by-step analysis of the lateral variation of the Vs parameter and is illustrated in figure 10. The first

step of the methodology consists of extracting the Vs parameter at a given depth in marly limestone. To do this for each segment, a depth of -10 m below the calibrated or assumed top of marly limestone was chosen to ensure that the extraction is reliable and representative of the marly limestone lithology Vs values. Next, an absolute difference (dVs) relative to the average Vs value of each segment at this depth was computed. This step eliminates large-scale Vs variations associated with changes in the lithology and allows retention of only local changes in the parameter. Smooth dVs curves were then obtained by applying a 10 m moving average filter to eliminate variations induced by 2D interpolation of Vs profiles. Finally, an extraction of negative dVs values was made. In the end, this step allows the identification of areas that highlight lower mechanical parameters than the mean of the segment.

The statistical evaluation of dVs values over the entire studied area allows merging these values in a histogram (Fig. 11) representing their occurrence frequency according to the dVs classes. Such an analysis permits identifying 3 groups of different dVs, each most likely linked to different weathering steps of limestone during the karstification process. Based on these three groupings, karst presence probability was assigned a level of 1 for dVs ranging from -10 to -45 m/s, 3 for dVs ranging from -45 to -95 m/s and 5 for dVs over -95 m/s. Values of dVs above -10 m/s were not taken into account.

7. Assessing sinkhole susceptibility: a combined interpretation

All the dykes were built on the alluvial floodplain of the Loire River. The thickness of the alluvial deposits is therefore an important parameter to take into account, as it can have a significant impact on the stability of these structures. Indeed, the thicker the alluvial cover, the more it will be able to fill any karst voids and thus attenuate the effect at the base of the dyke. Conversely, if the cover is thin, the filling of karst voids will only be partially provided by the alluvial cover, and the body of the dykes will be exposed to disorders.

The complementary use of MASW and ERT investigations allows highlighting multiple correlated Vs and resistivity anomalies on the segments, which may correspond to different stages of sinkhole propagation from the deep karst network to the surface through the alluvial cover (Figs. 12 to 14).

In the western part of the segment shown in figure 12a, a low Vs anomaly, most likely due to the presence of a karst network in depth, is identified. In addition, neither electrical flow anomalies nor historical karst-related surface disorders are observed in line with this Vs anomaly. Hence, this case highlights the development of a karstification process at the top of the marly limestone formation, without any impact on the overlying materials, and can be represented via the conceptual diagram of figure 12b.

Between abscissa -550 and -150 m of the segment shown in figure 13a, a vast low Vs anomaly, most likely due to the presence of a karst network in depth, is identified. This anomaly has good consistency with electrical flow anomalies observed in the alluvial deposits at the same abscissa. On the other hand, no karst-related surface disorders were identified in this area of the BD. This case could correspond to a flow of alluvial materials into an existing deep karst system (Fig. 13b). This type of scenario highlights a potential future collapse area.

At the centre of the segment shown in Figure 14a, 3 low Vs anomalies, most likely due to the presence of karst networks in depth, are identified. These anomalies have good consistency with electrical flow anomalies observed in the alluvial deposits, and many historical karst-related surface disorders with karst origins (BD) are in line with these Vs anomalies. This type of scenario highlights the final stage of a karst sinkhole (Fig. 14b).

Although electric investigations performed with the OhmMapper system do not reach the marly limestone bedrock where karstification occurs, some resistivity anomalies affecting the underbody of the dyke are likely to mark not only the possible presence of karst but also

their consequences on near-surface formations. Potential collapse of these formations is demonstrated by patterns of sediment flow into the karst system. Thus, flowing sediment electrical anomalies affecting the underbody of the dike, linked to a strong karst presence probability extracted from Vs values may be reported as future collapse areas and constitute a good indicator for the assessment of sinkhole susceptibility. However, the electrical resistivity is known to be quite sensitive to the nature of the geological formation (clay content, water content, sand etc.). As mentionned in the section 4 through the calibration of the electrical cross-sections, resistivities are relevant for different types of alluvial deposits (from conductive clayey sediments to resistive sand and gravels). Resistivity values linked to the flowing sediment electrical anomalies can thus not be uniquely related to a weathering index or to the intensity of a sinkhole phenomenon but rather to the nature of the sediment which flows to the depth.

A statistical index extracted from the resistivity data of the electrical anomalies would doubtless more highlight geological changes in the flowing sediments than changes in the intensity of the sinkhole phenomenon. A sinkhole occurrence susceptibility level was then derived considering only a conditional index 0 or 1 according to the presence or not of an electrical anomaly (Fig. 15). An index of 1 was then added to the karst presence susceptibility level where flowing sediment electrical anomalies are identified and 0 was added elsewhere. Assessing the sinkhole susceptibility level over the entire set of investigated segments then became possible (Fig. 12, 13, 14 and 16a).

8. Discussion and Conclusion

To assess the reliability of the methodology, the obtained sinkhole susceptibility level was interpolated using a kriging technique over the entire set of investigated segments to obtain a

sinkhole susceptibility map. The map shows sinkhole susceptibility on an empirical scale based on geophysical indicators. It is first compared to the projected karst-related surface disorders on the dykes from the BD cavités (Fig. 16a). Karstic caves in plan view resemble ink blots or Rorschach patterns. Ramiform irregular cavities and galleries wander three-dimensionally with branches extending outward, up to possibly hundred meters, from the main areas of development (Palmer, 1991). Thereby, assuming that a disorder related to the same karstic network will not necessarily appear directly on the measured line, a search area of 100 m was used for the interpolation and as a buffer area on either side of dykes for the selection of database events. There is an acceptable consistency between areas of high sinkhole susceptibility and the projected locations of karst-related surface disorders, 60 % of them being located in high susceptibility areas (≥ 2). This provides a consistency check of the sensibility of the methodology to karst phenomena, although the susceptibility level should be more related to the prediction of future disorders than to the detection of former ones. Secondly, the sinkhole susceptibility map is compared to the projected sinkholes extracted from the French National database of land movements (BD mvt) which occurred after 2008, i. e. after the acquisition of geophysical data (Fig 16a). Here again, a buffer area of 100 m on either side of dykes was used for the selection of database events. One can see that there is a better correlation between these two elements, 86% of the sinkholes which occured after the geophysical survey being located within high susceptibility areas (≥ 2) (Fig. 16c). Hence, it appears too that some areas which were not disturbed at the time of the geophysical acquisition, especially at the north of St-Pryvé-St-Mesmin city and at the north-east of Sandillon city, present sinkholes few years later. This observation highlights the effective ability of the methodology to predict areas of potential future collapse and provides a reliability check of the presented sinkhole susceptibility map. However, this statistical analysis should be carefully interpreted according to the few number of sinkholes which

occurred after the geophysical survey. Let's note that the low and very low susceptibility categories do not indicate that sinkholes have not or cannot occur in these areas as shown by the sinkhole that occured after the geophysical survey at the east of the Sandillon city in an area of low sinkhole susceptibility level. This could be explained by the variability of the collapse phenomenon kinetics, the sudden occurrence of a sinkhole due to a surficial layer breaking being undetectable by the methodology based on the presence of precursor resistivity anomalies near the surface.

As a consequence, a limitation of the susceptibility map is the possibility that other causative factors not considered in our analysis may result in sinkhole occurence. Local hydrology and precipitations are two of these factors. This map is not intended for use at scales other than the published scale and such use may result in erroneous conclusions regarding sinkhole hazard. The map is designed for regional planning use to determine areas where local sinkhole hazards may exist on the dykes and where more detailed planning maps and geotechnical studies are needed, particularly in areas of high and moderate susceptibility.

ERT and MASW coupling is a promising approach to detecting and characterising karst structures in urban environments, with the two methods being complementary in depth of investigation and origin of detected anomalies. MASW surveying was effective at mapping the interface between overburden alluvial deposits and the marly limestone bedrock. MASW surveys successfully highlighted zones of low velocity and therefore mechanical weaknesses corresponding to karstified areas in limestones. Such detection allowed the assessment of a karst presence probability level with a better resolution (10 m) than former studies in the same area. For comparison, Donsimoni et al. (2008) estimated karst presence probability over the entire Loire River and especially in the study area with a resolution of 500 m using 3 indirect geological and hydrogeological indicators: the sensibility of the substratum to the dissolution phenomenon according to its nature, structure and fracturation degree criteria, the

thickness of the alluvial sedimentary cover and the water circulation mode between the alluvial and karst aquifer. In addition to the resolution, the exposed methodology also has the advantage of providing a probability level based on direct observations of the subsurface state, making the evaluation more reliable.

Resistivity surveying at the top of the dykes was also useful to detect potential flow of near-surface materials into karst at depth. By integrating results obtained using these two geophysical techniques, it was possible to highlight areas of interaction between karst and the near-surface formations that were previously poorly understood. Providing this characterization of near surface materials using the resistivity survey, the integrated results allowed evaluating a sinkhole susceptibility empirical level at the field scale which confers to the methodology its predictive purpose in opposition to the usual characterization aim of geophysical applications. This non-intrusive, rapid and inexpensive approach seems promising for mapping long segments of river dykes and aid engineers in predicting any potential dangers or hidden hazards.

Acknowledgments

We thank the LRPC Blois (Laboratoire Régional des Ponts et Chaussées) for having made available their geotechnical surveys of the Loire River dykes. We also thank the DREAL Centre (Direction Régionale de l'Environnement, de l'Aménagement et du Logement) for providing useful information to the geophysicists. We are very grateful to the BRGM technicians for their field work. This work was supported by BRGM-DREAL Centre public research program 2006-CEN-18. We thank the anonymous reviewers for their constructive comments which helped to improve the manuscript.

References

Aki, K., Richards, P.G., 1980. Quantitative Seismology. W.H. Freeman and Company, San Francisco.

Benson, A.K., Payne, K.L., Stubben, M.A., 1997. Mapping groundwater contamination using DC resistivity and VLF geophysical methods—A case study. Geophysics 62, 80-86.

BD cavités: French National database of underground cavities. www.bdcavite.net

BD mvt: French National database of land movements. www.bdmvt.net

Beres, M., Luetscher, M., Olivier, R., 2001, Integration of ground-penetrating radar and microgravimetric methods to map shallow caves. J. Appl. Geophys. 46, 249-262.

Bitri, A., Jousset, P., Samyn, K., Naylor, A., 2010. River dykes investigation and effects of the topography on seismic surface waves propagation. Proceedings of the EGU General Assembly 2010, May 2-7, 2010, Vienna, Austria, p.4777.

Bobatchev, A.A., 2003. X2IPI software: http://geophys.geol.msu.ru/x2ipi/x2ipi.html Chen, C., Liu, J., Xia, J., Li, Z., 2006. Integrated geophysical techniques in detecting hidden dangers in river embankments. J. Environ. Eng. Geoph. 11, 83-94.

Dahlin, T., Zhou, B., 2004. A numerical comparison of 2D resisitivity imaging with 10 electrode arrays. Geophysical Prospecting, 2004, 52, 379-398.

Debeglia, N., Bitri, A., Thierry, P., 2006. Karst investigation using microgravity and MASW: application to Orléans, France. Near Surf. Geophys. 4, 215-225.

Donsimoni, M., Berthier, H., Martin, J.-C., Nachbaur, A., 2008. Détermination de la présence de karst sous les levées domaniales du bassin de la Loire et réduction du risque d'effondrement de la digue lié à la présence de ces conduits souterrains naturels. Tranche 1: analyse géologique et hydrogéologique. Rapport final. BRGM/RP-55711. http://pmb.brgm.fr/brgm/brgm_broogle_notice.php?id=54092

Ford, D.C., Williams, P., *Karst Hydrogeology and Geomorphology*, John Wiley and Sons Ltd., 2007, ISBN 978-0-470-84996-5

Gabriels, P., Sneider, R., Nolet, G., 1987. In-situ measurements of shear wave velocity in sediments with higher mode Rayleigh waves. Geophys. Prospect. 35, 187-196.

Ganji, V., Gucunski, N., Maher, A., 1997. Detection of underground obstacles by SASW method-numerical aspects. J. Geotech. Geoenviron. Eng. 123, 212-219.

Geometrics, 2001. OhmMapper TR1 operation mannual (San Jose, CA).

Guerin, R., Benderitter ,Y., 1995. Shallow karst exploration using MT-VLF and DC resistivity methods. Geophys. Prospect. 43, 635-653.

Gunn, J., 2004, Encyclopedia of Caves and Karst Science. New York: Fitzroy Dearborn, 902p.

Hermann, R.B., 1987. Computer Programs in Seismology. Department of Earth and Atmospheric Sciences, St. Louis University, St. Louis, MO.

Ioannis, F.L., Filippos, I.L., Bastou, M., 2002. Accurate subsurface characterization for highway applications using resistivity inversion methods. Journal of Electrical and Electronics Engineering, Special Issue, October 2002, 43-55.

Johansson, S., Dahlin, T., 1996. Seepage monitoring in an earth embankment dam by repeated resistivity measurements. European Journal of Environmental and Engineering Geophysics 1, 229-247.

Karl, L., Fechner, T., Schevenels, M., François, S., Degrande, G., 2011. Geotechnical characterization of a river dyke by surface waves. Near Surf. Geophys. 9, 515-527.

Kaufmann, O., 2000. Les effondrements karstiques du Tournaisis : genèse, évolution, localisation, prévention. Thèse 3ème cycle, Faculté Polytechnique de Mons (Belgique).

Khair, K., Skokan, C., 1998. A model study of the effect of salination on groundwater resistivity. J. Environ. Eng. Geoph. 2, 223-231.

Leparoux, D., Bitri, A., Grandjean, G., 2000. Underground cavity detec-tions: a new method based on seismic Rayleigh waves. European Journal of Environmental and Engineering Geophysics 5, 33-53.Lino, M., Mériaux, P., Royet, P., 1999. Méthodologie de diagnostic des digues appliquée aux levées de la Loire moyenne. Antony, Hauts-de-Seine. Antony (92), Cemagref Éditions, 1999 (ISBN 2-85362-524-9)

Loke, M.H., Acworth, I. and Dahlin, T., 2003. A comparison of smooth and blocky inversion methods in 2D electrical imaging surveys. Exploration Geophysics, **34**, 182-187. (IF 0.619)

Loke, M.H. and Dahlin, T., 2002. A comparison of Gauss-Newton and quasi-Newton methods in resistivity imaging inversion. Journal of Applied Geophysics, **49**, 149-162. (IF 1.185)

McMechan, G.A., Yedlin, M.J., 1981. Analysis of dispersive waves by wave field transformation: Geophysics 46, 869-874.

Matthews, M.C., Hope, V.S., Clayton, R.I., 1996. The use of surface waves in the determination of ground stiffness profiles. P I Civil Eng-Geotec 119, 84-95.

Miller, R.D., Xia, J., Park, C.B., Ivanov, J., 1999. Multichannel analysis of surface waves to map bedrock. The Leading Edge 18, 1392-1396.

Moktar, T.A., Herrmann, R.B., Russel, D.R., 1988. Seismic velocity and Q model for the shallow structure of the Arabian shield from short period Rayleigh waves. Geophysics 53, 1379-1387.

Palmer, A.N., 1991, Origin and morphology of limestone caves, Geological Society of America Bulletin, v. 103, p 1-21.

Park, C.B., Miller, R.D., Xia, J., 1999. Multichannel analysis of surface-waves. Geophysics 64, 800-808.

Park, C.B., Xia, J., Miller, R.D., 1998. Ground roll as a tool to image near-surface anomaly. 68th SEG Meeting, New Orleans, LA, Expanded Abstracts, pp. 874-877.

Saksa, P., Paananen, M., 1992. Case study: mapping of groundwater conditions at Olkiluoto site with electrical and electromagnetic boreholes. 54th Meeting of the European Association of Exploration Geophysics, pp. 694-695.

Sandberg, S.K., 1993. Examples of resolution improvement in geoelectrical boreholes applied to groundwater Investigations. Geophys. Prosp. 41, 207-228.

Shtivelman, V., 2002. Surface wave section as a tool for imaging subsur-face inhomogeneities. European Journal of Environmental and Engineering Geophysics 7, 121-138.

Sjo¨dahl, P., Dahlin, T., Johansson, S., 2003. Resistivity monitoring for leakage detection at Ha¨llby embankment dam. Proceedings of the 9th Meeting Environmental and Engineering Geophysics, Prague, Czech Republic, 31 August–4 September 2003, O 015, p. 4.

Socco, L.V., Strobbia, C., 2004. Surface-wave method for near-surface characterization: a tutorial. Near Surf. Geophys. 2, 165-185.

Valois, R., Bermejo, L., Guérin, R., Hinguant, S., Pigeaud, R., Rodet, J., 2010. Karst morphologies identified with geophysics around Saulges caves (Mayenne, France). Archaeol. Prospect. 17, 151-160.

Valois, R., Camerlynck, C., Dhemaied, A., Guérin, R., Hovhannissian, G., Plagnes, V., Rejiba, F., Robain, H., 2011. Assessment of doline geometry using geophysics on the Quercy plateau karst (South France). Earth Surf. Proc. Land. 36, 1183-1192.

van der Veen and Green, 1998 Land streamer for shallow seismic data acquisition: evaluation of gimbal mounted geophones, Geophysics, 63, 1408-1413.

Xia, J., Chen, C., Li, P.H., Lewis, M.J., 2004. Delineation of a collapse feature in a noisy environment using a multichannel surface wave technique. Geotechnique 54, 17-27.

Xia, J., Chen, C., Tian, G., Miller, R.D., Ivanov, J., 2005. Resolution of high-frequency Rayleigh-wave data. Journal of Environmental and Engineering Geophysics, Special Issue on Seismic Surface Waves 10. 99-110.

Xia, J., Miller, R.D., Park, C.B., 1998. Construction of vertical section of near-surface shear-wave velocity from ground roll. Technical Program, The Society of Exploration Geophysicists and The Chinese Petroleum Society, Beijing '98 International Conference, pp. 29-33.

Xia, J., Miller, R.D., Park, C.B., 1999. Estimation of nearsurface shear-wave velocity by inversion of Rayleigh wave. Geophysics 64, 691-700.

Xia, J., Miller, R.D., Park, C.B., Hunter, J.A., Harris, J.B., Ivanov, J., 2002b. Comparing shear-wave velocity profiles from multichannel analysis of surface-wave with borehole measurements. Soil Dyn. Earthq. Eng. 22, 181-190.

Xia, J., Miller, R.D., Park, C.B., Tian, G., 2002a. Determining Q of near-surface materials from Rayleigh waves. J. Appl. Geophysi. 51, 121-129.

Xia, J., Miller, R.D., Park, C.B., Tian, G., 2003. Inversion of high frequency surface-waves with fundamental and higher modes. J. Appl. Geophys. 52, 45-57.

Xia, J., Miller, R.D., Park, C.B., Wightman, E., Nigbor, R., 2002c. A pitfall in shallow shear-wave refraction surveying. J. Appl. Geophys. 51, 1-9.

Figure captions

Figure 1: Karst presence probability map near the city of Orléans (adapted from Donsimoni et al., 2008). The study area is represented by the red rectangle.

Figure 2: a) Location map of the study area showing geophysical profiles in black solid lines. Geophysical sections shown in the referred figures of the paper are highlighted using red and green solid lines respectively for the resistivity sections and the Vs sections.

Figure 3: Photography of a sinkhole at the top of a Loire River dyke.

Figure 4: ERT typical a) raw and b) filtered apparent resistivity pseudo-section obtained on a segment of the Loire River dykes; depths of available apparent resistivity data using the acquisition configuration overlay the sections in black dotted lines, c) MASW typical seismic shot records and d) the corresponding dispersion diagrams obtained on 3 different segments of the Loire River dykes.

Figure 5: Typical examples of electrical resistivity calibration for the clayey silt (a), clayey sand (b) and sandy gravel (c) lithologies. The lithological description of the destructive soundings is compared to the inverted resistivity section at the same location. RMS errors between measured and modeled apparent resistivity values correspond to the entire profile from which the sections are extracted.

Figure 6: Typical examples of interpreted electrical resistivity sections, highlighting resistivity anomalies. Historical karst-related surface disorders, available in the BD cavités, are marked using black arrows and are followed by the projection distance of the disorder

location on the dykes (in metres). RMS errors between measured and modeled apparent resistivity values correspond to the entire profile from which the segments are extracted.

Figure 7: Typical examples of interpreted electrical resistivity sections, highlighting sudden change in resistivity and turning-down patterns at the base of the dyke bodies. These anomalies are likely to correspond to areas of potential sediment flow toward a karst network. RMS errors between measured and modeled apparent resistivity values correspond to the entire profile from which the segments are extracted.

Figure 8: Typical examples of Vs calibration. The lithological description of the destructive soundings is compared to the Vs section at the same location.

Figure 9: Typical examples of interpreted MASW sections. Vs anomalies highlight potential karstified areas at the top of the marly limestone. Historical karst-related surface disorders, available in the BD cavités, are marked using black arrows and are followed by the projection distance of the karst-related surface disorders location on the dykes (in metres). The interface between the overburden deposits and the marly limestone overlay the sections in black dotted lines. The delineation of interpreted karst features overlay the section in black solid lines.

Figure 10: successive steps of the karst presence probability assessment methodology. a) Typical MASW section presenting Vs anomalies at the top of the marly limestone. The Vs values' extraction depth is marked with a black solid line, b) extracting Vs values, c) computed absolute difference dVs relative to the average Vs value for the segment at the extraction depth, d) smoothed dVs, obtained using a 10 m moving average filter, e) negative dVs, highlighting lower mechanical parameters than the mean of the segment and f)

computed probability of karst presence level for the segment according to the dVs statistical distribution.

Figure 11: Histogram of dVs values in the entire studied area. The statistical Gaussian distribution exhibits 3 groups of different dVs, each most likely linked to different weathering steps of limestone during the karstification process.

Figure 12: a) An example of correlations between the Vs and electrical resistivity section on the same segment. The RMS error between measured and modeled apparent resistivity values correspond to the entire profile from which the segments is extracted. Historical karst-related surface disorders, available in the BD cavités, are marked using black arrows. The projection distance of the disorder location on the dyke (in metres) is also indicated. The karst presence probability level and the electrical resistivity anomaly index for this segment are presented as colour bars between the two sections. In the western part of the segment, a low Vs anomaly, most likely due to the presence of a karst network in depth, is identified. In addition, neither electrical flow anomalies nor historical karst-related surface disorders are observed in line with this Vs anomaly. This case highlights the b) conceptual view of the development of a karstification process at the top of the marly limestone formation, without any impact on the overlying materials.

Figure 13: a) An example of correlations between the Vs and electrical resistivity section on the same segment. The RMS error between measured and modeled apparent resistivity values correspond to the entire profile from which the segments is extracted. The karst presence probability level and the electrical resistivity anomaly index for this segment are presented as colour bars between the two sections. Between abscissa -550 and -150 m of the segment, a

vast low Vs anomaly, most likely due to the presence of a karst network in depth, is identified. This anomaly has good consistency with electrical flow anomalies observed in alluvial deposits at the same abscissa. In contrast, no karst-related surface disorders were identified in the BD in this area. This case could correspond to b) the conceptual view of the flow of alluvial materials into an existing deep karst system. This type of scenario highlights a potential future collapse area.

Figure 14: a) An example of correlations between the Vs and electrical resistivity section on the same segment. The RMS errors between measured and modeled apparent resistivity values correspond to the entire profile from which the segment is extracted. Historical karst-related surface disorders, available in the BD cavités, are marked using black arrows. The projection distance of the disorder location on the dyke (in metres) is also indicated. The karst presence probability level and the electrical resistivity anomaly index for this segment are presented as colour bars between the two sections. At the centre of the segment, 3 low Vs anomalies, most likely due to the presence of karst networks at depth, are identified. These anomalies have good consistency with electrical flow anomalies observed in the alluvial deposits, and many historical karst-related surface disorders with karst origins (BD) are in line with these Vs anomalies. This type of scenario highlights the b) conceptual view of the final stage of a karst sinkhole.

Figure 15: a) An example of the karst presence probability level obtained along the segment shown in figure 10. The associated electrical resistivity anomaly conditional index overlays the plot in the red solid line. One can observe the consistency between these two indices. b) The associated sinkhole susceptibility level obtained by incrementing the karst presence probability level using the electrical resistivity anomaly conditional index.

Figure 16: a) Sinkhole susceptibility map interpolated over the entire set of investigated segments. Historical karst-related surface disorders, available in the BD cavités, are marked using black dots. Sinkholes which occurred after 2008, available in the BD mvt, are marked using green dots. b) Distribution of the karst-related surface disorder according to the mean sinkhole susceptibility level. c) Distribution of the sinkholes which occurred after 2008 according to the mean sinkhole susceptibility level. One can see the good correlation between high susceptibility areas and sinkholes which occur after the geophysical survey. This observation highlights the ability of the methodology to predict areas of potential future collapse and provides a reliability check of the sinkhole susceptibility map.

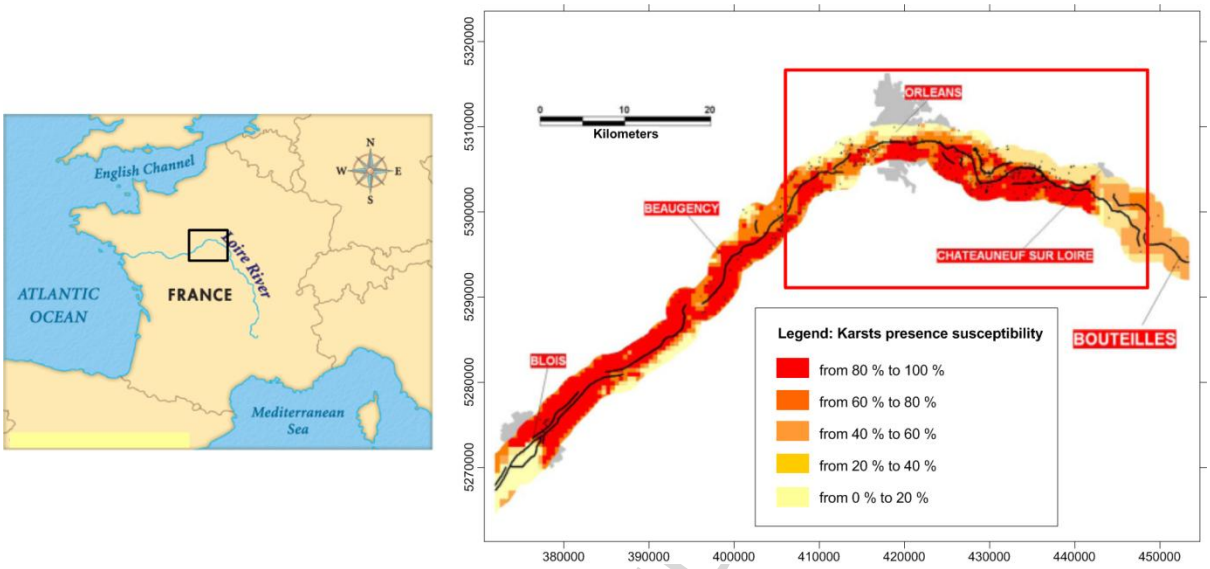

Figure 1

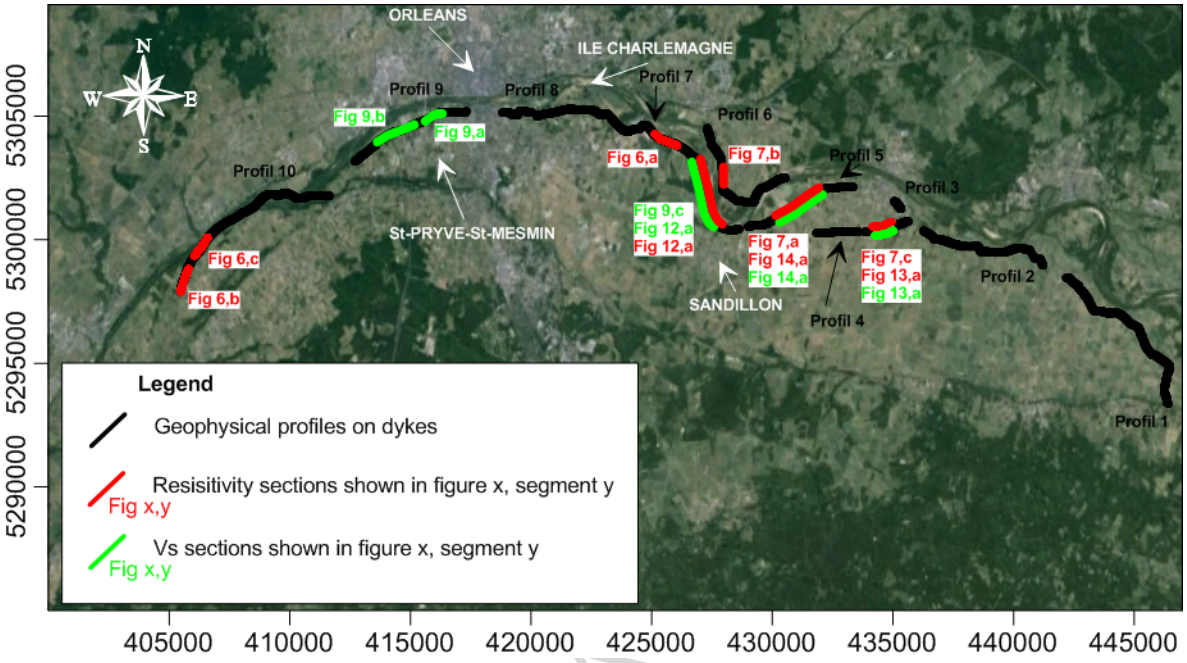

Figure 2

Figure 3

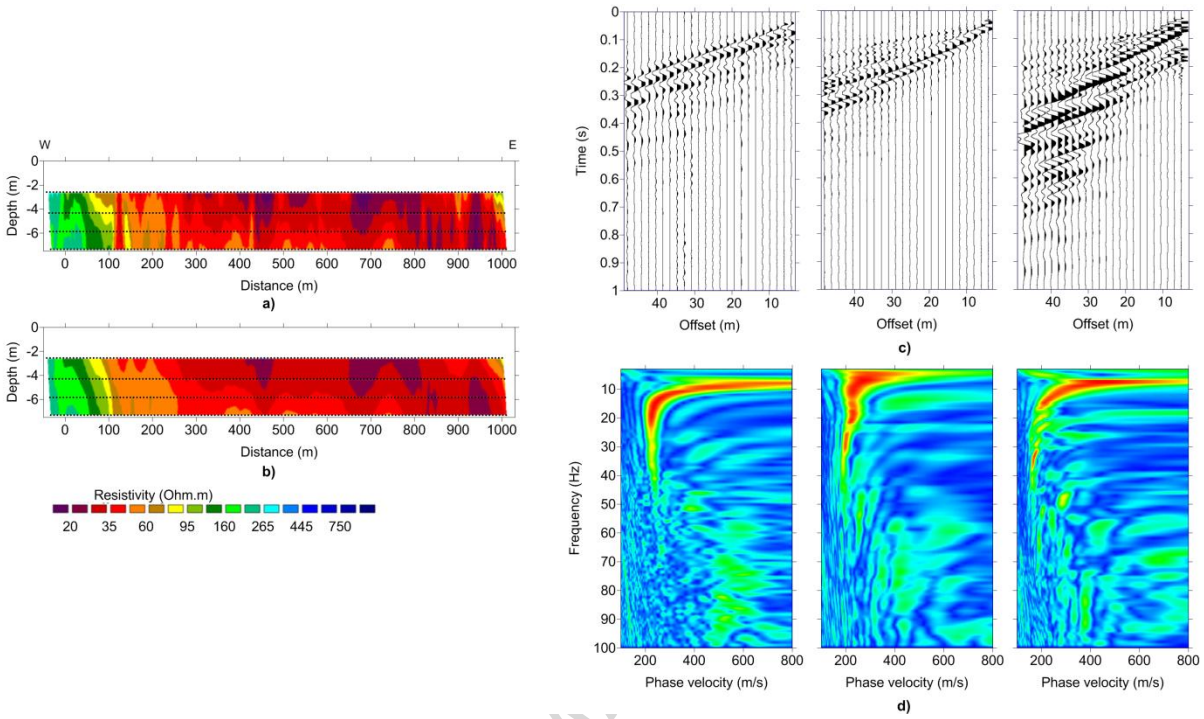

Figure 4

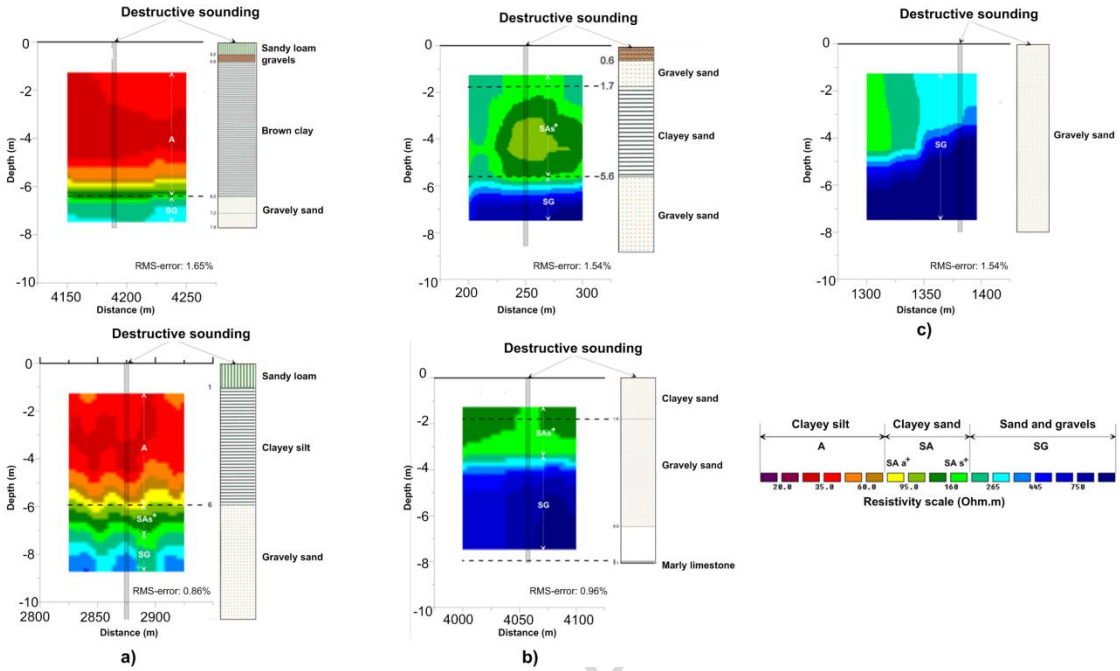

Figure 5

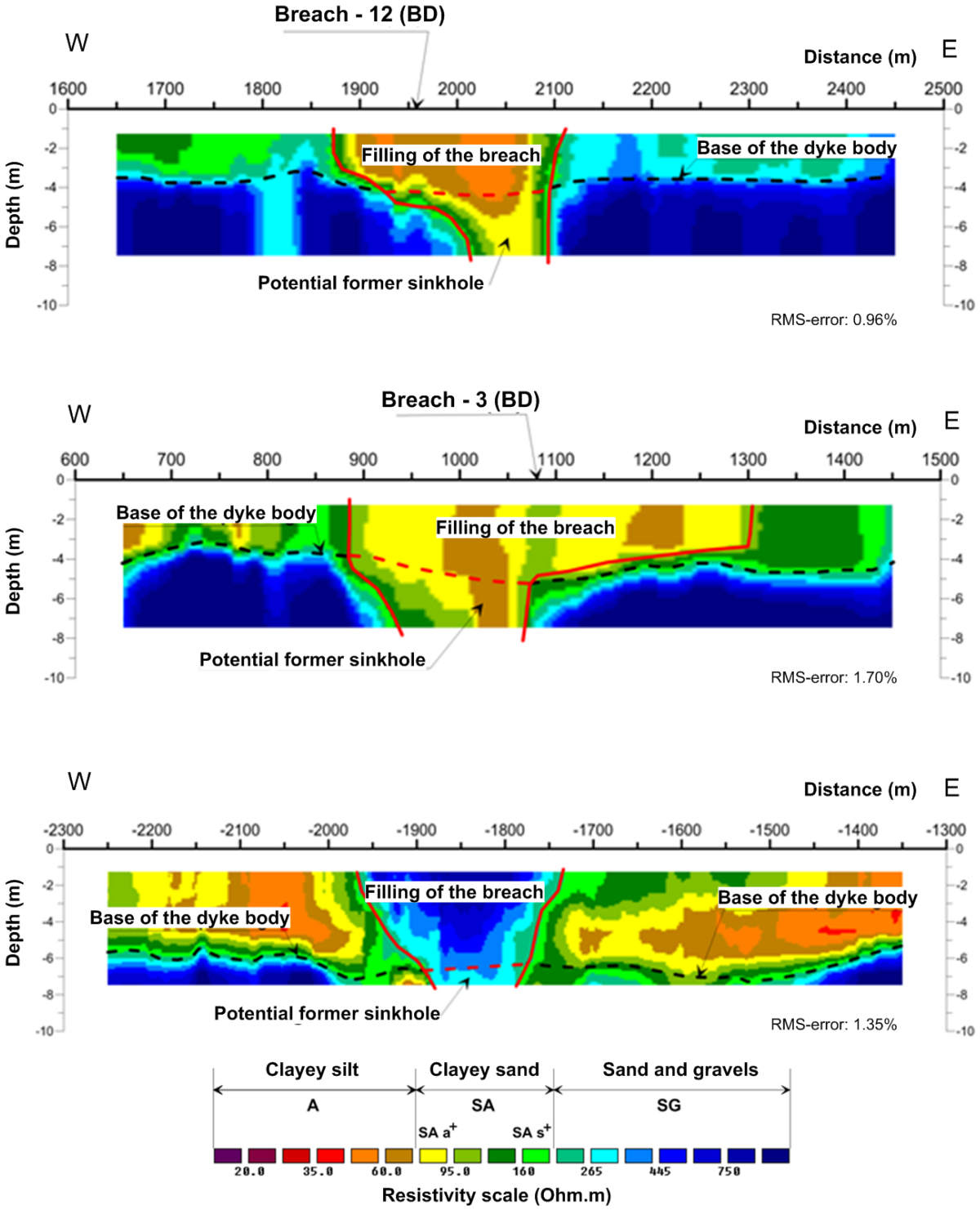

Figure 6

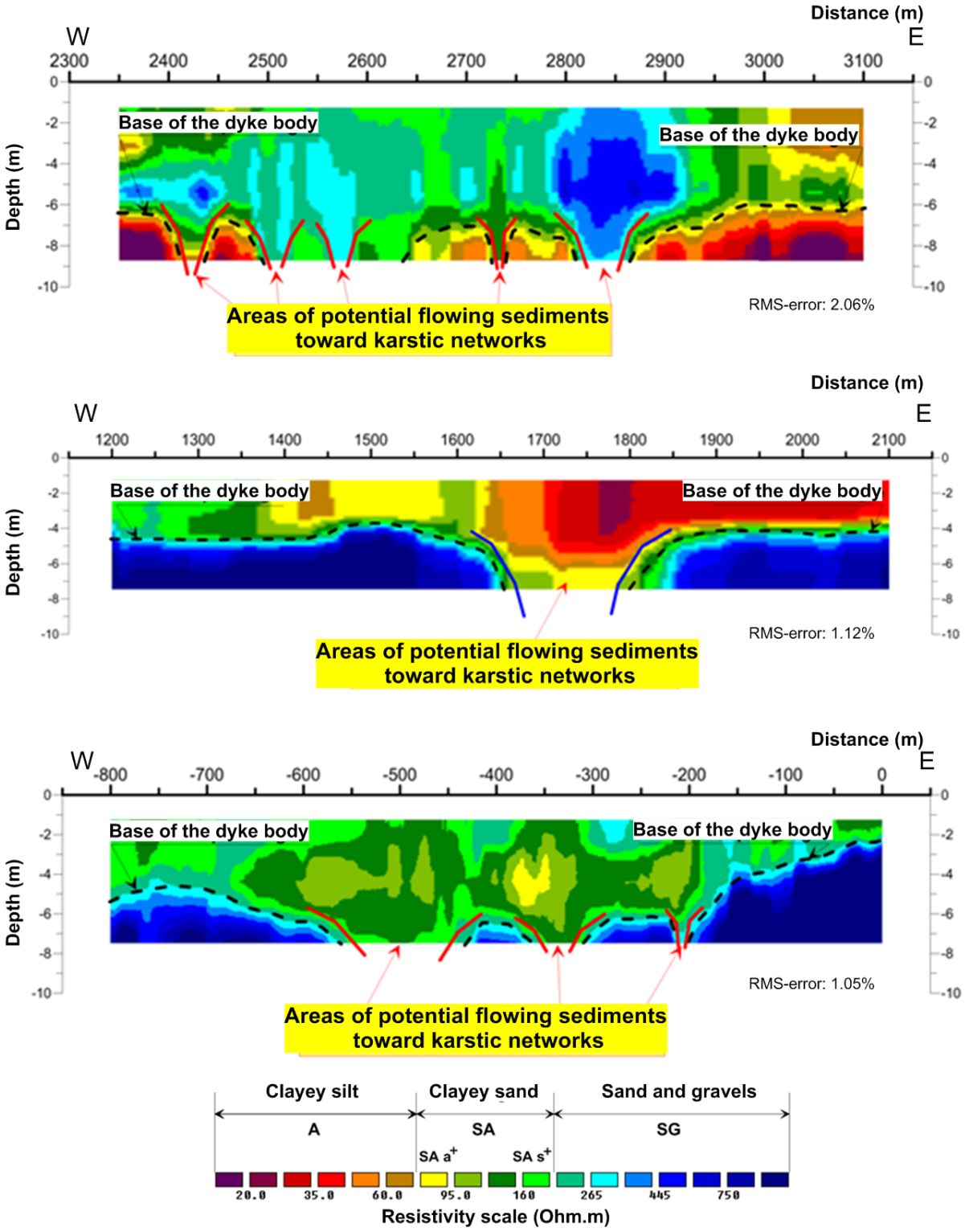

Figure 7

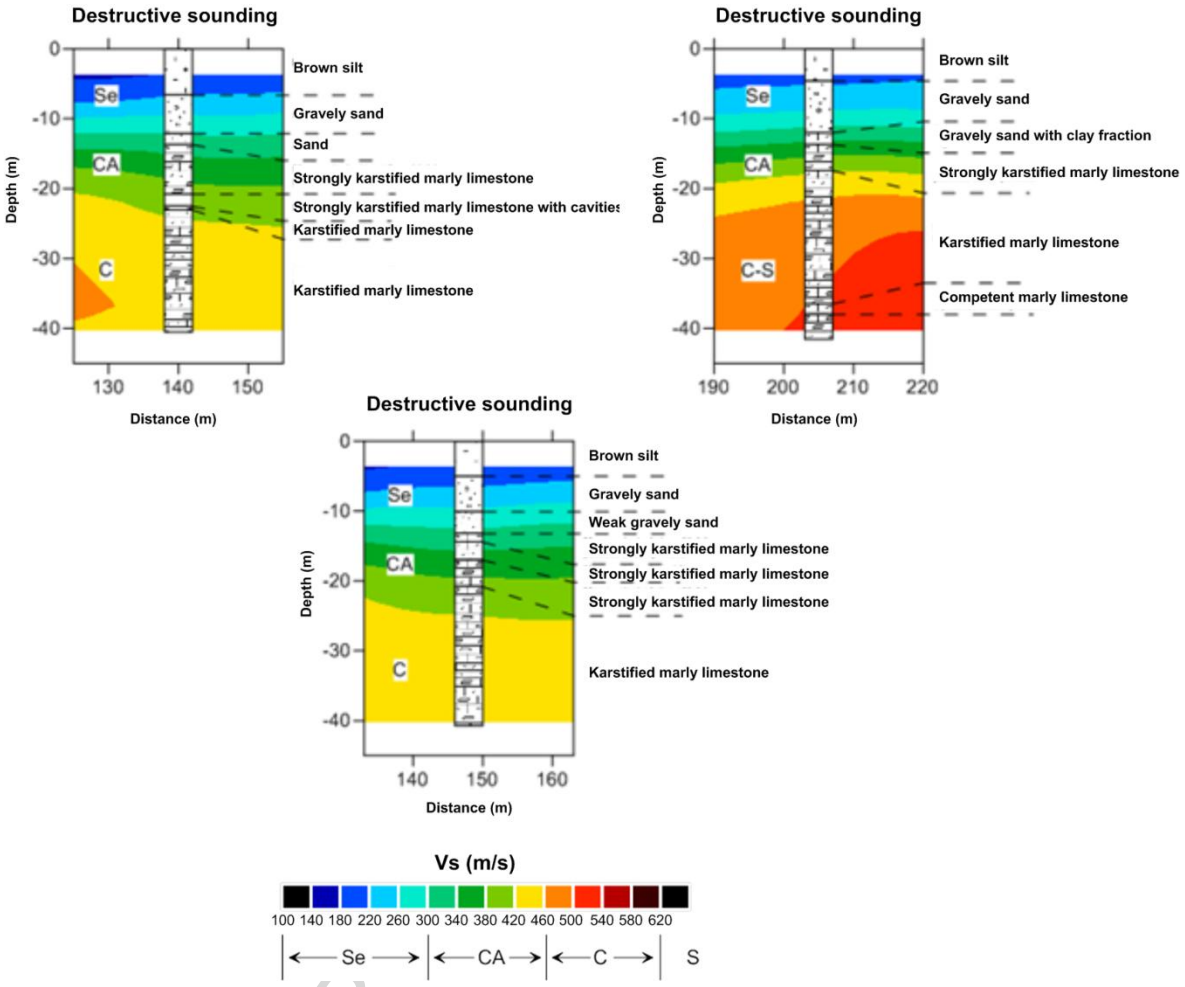

Figure 8

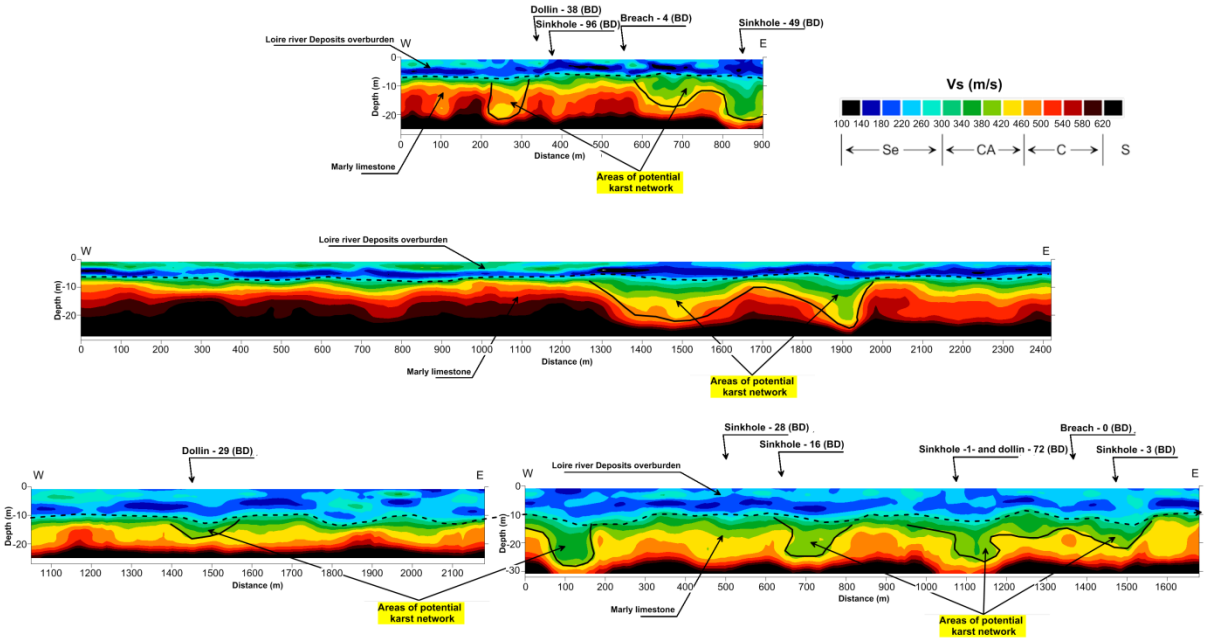

Figure 9

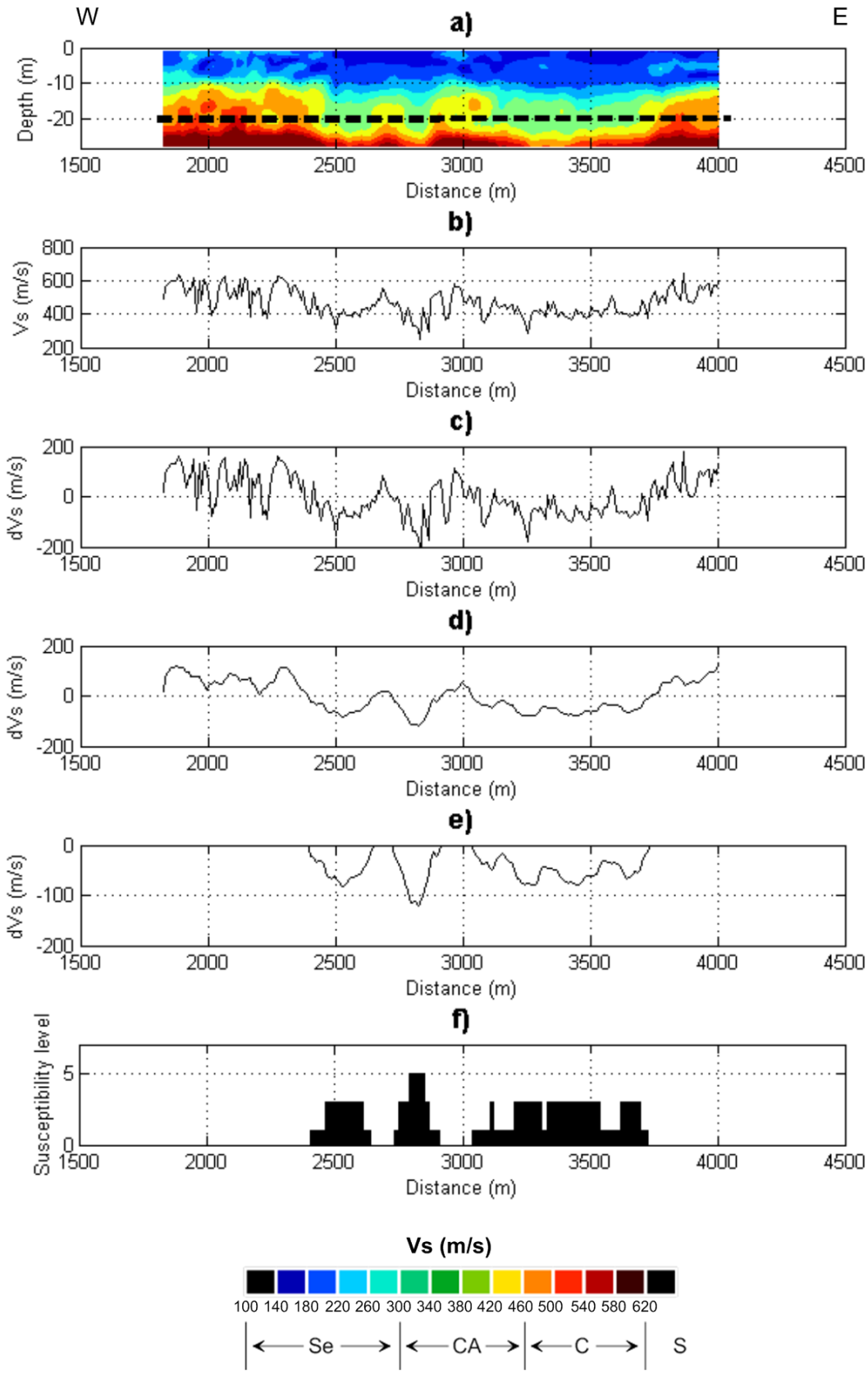

Figure 10

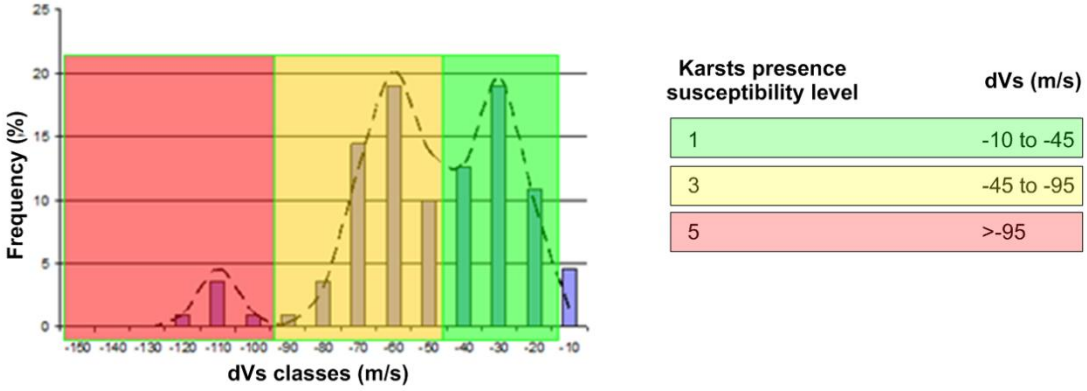

Figure 11

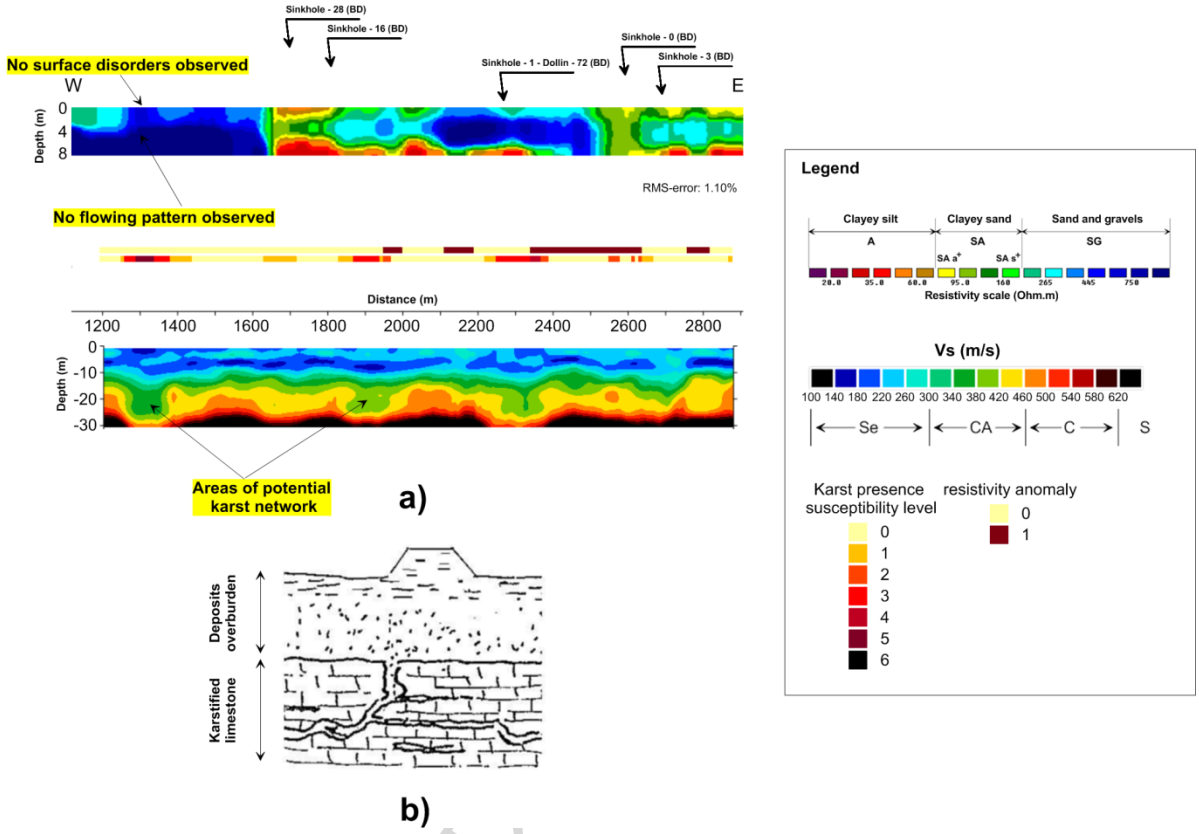

Figure 12

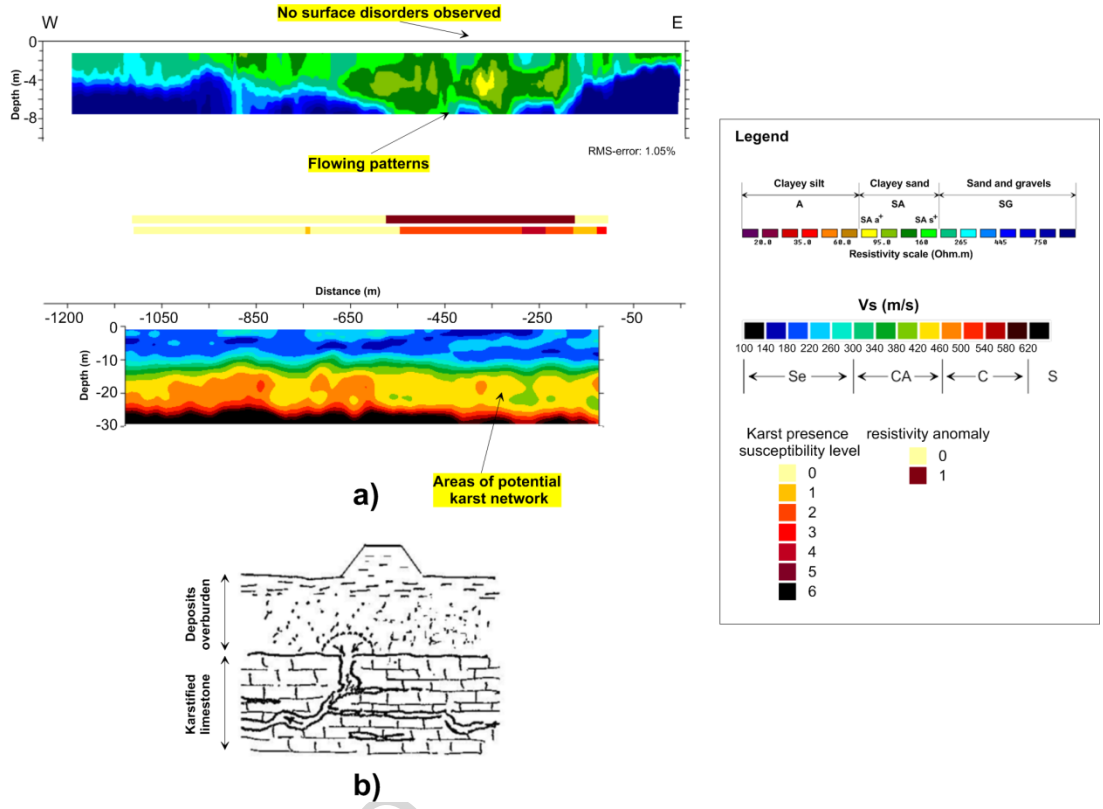

Figure 13

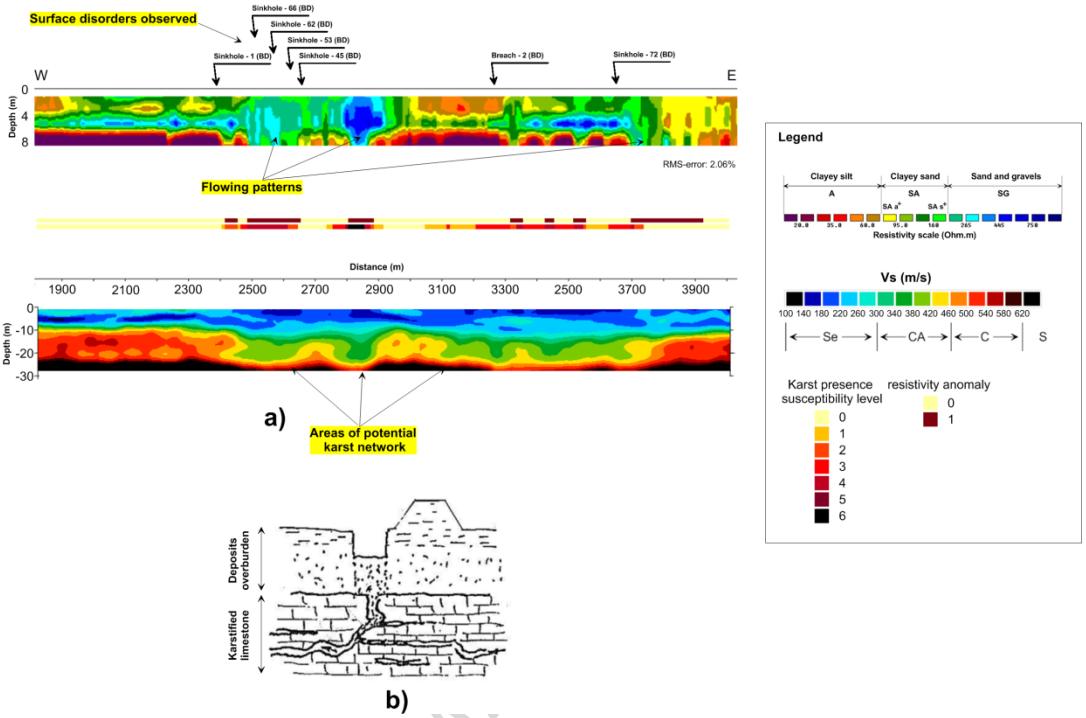

Figure 14

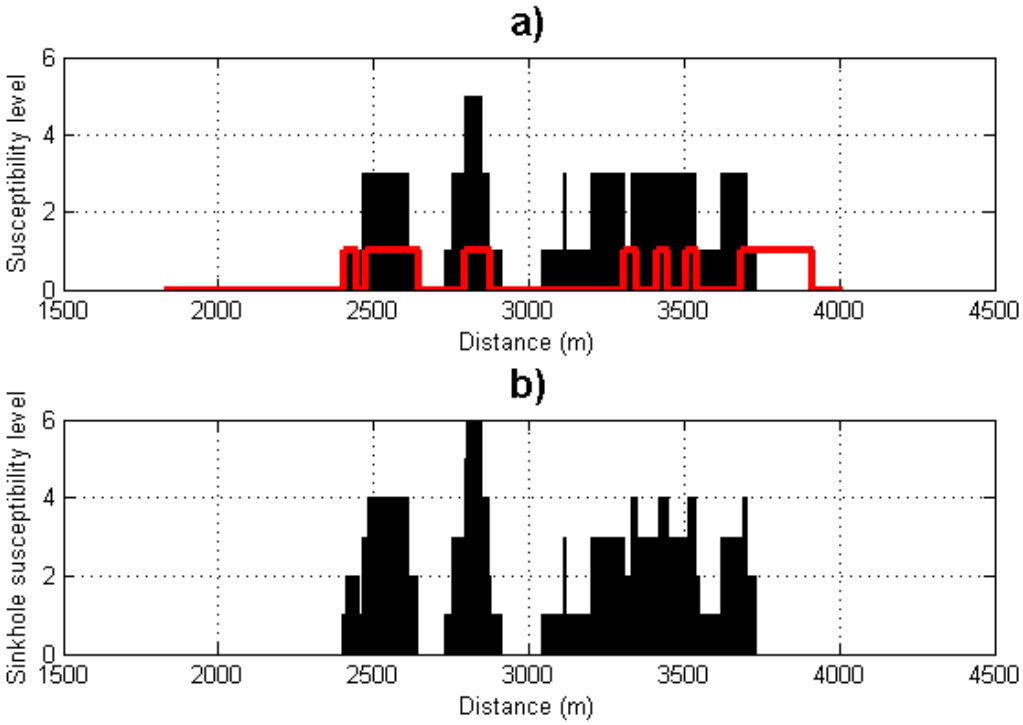

Figure 15

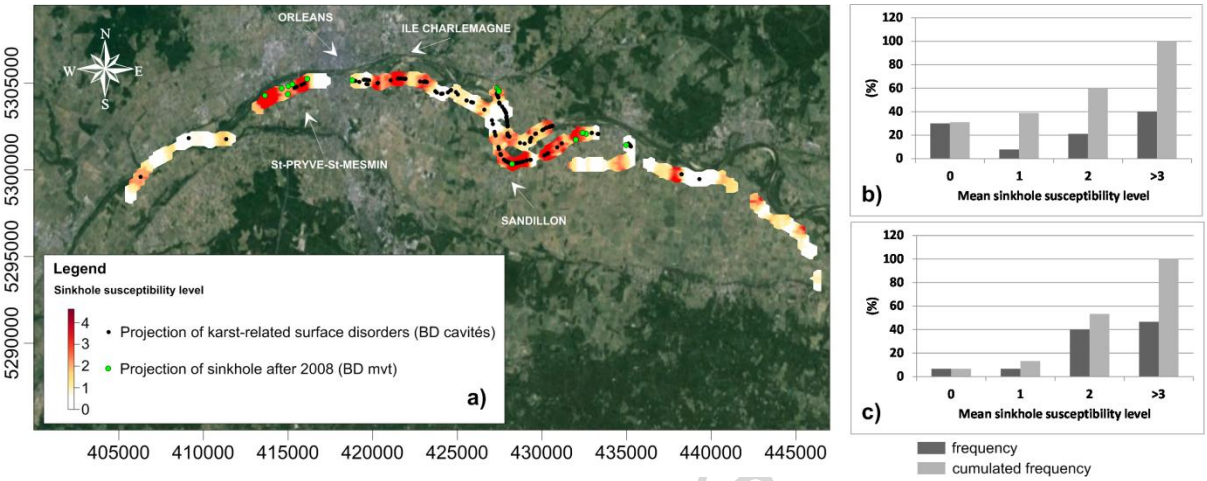

Figure 16

Highlights

- A series of geophysical experiments were conducted to detect karst features below a dyke system
- The mapping of weak areas in limestone allowed the assessment of a karst presence probability level
- Resistivity surveying was useful to detect potential flow of near-surface materials into karsts
- By integrating results, interaction between karsts and the near-surface formations was highlighted
- It then allowed mapping of these sinkhole-susceptible areas with a better accuracy than former studies